

On the Development of a Multi-Modal, Selectively Lockable, Compact, Affordable Knee Joint Assembly for Bipedal Robots

Cheng-Yueh Liu¹, Jaspreet S. Dhupia¹, Minas Liarokapis¹, and Pei-Chun Lin²

Abstract—Contemporary advances in humanoid bipeds include complicated mechanisms supporting fully actuated robotics. While these solutions offer unprecedented versatility that relies on sophisticated locomotion systems, the efficient traversing capabilities of natural, passive-inspired gait may be overlooked. In this paper, we focus on the development of a disengage-able, selectively lockable, affordable knee joint assembly suitable for either active or underactuated biped operation. The multi-modal nature of the design facilitates actuated bidirectional rotation as well as disengaged operation, while the knee lock ensures legs remain rigid during stance phase. Experimental validation of the performance of the knee assembly demonstrated both controllable knee joint actuation and fully passive rotation, various modes of operation, and torque evaluations. Further investigations include validation testing of operational and locking performance on a physical bipedal robot. System parameter optimizations can reduce energy consumption. The design proved feasible and is open-sourced to facilitate replication and co-development with others.

I. INTRODUCTION

Bipedal robots are characterized by an unparalleled versatility, leveraging their advanced human-like locomotion capabilities that allow them to traverse dynamic and unstructured human-oriented environments. These systems must include a mechanism that reduces effective hip-foot length. A knee joint mechanism provides such capability in humanoids, which is essential to prevent foot scuffing during leg swing phase. The rear leg can rotate forward without the feet hitting the ground. However, many implementations try to achieve the most overpowered solution for utmost capability, which obfuscates elegance and basic requirements in simple bipedal gait. Through appreciating fundamental paradigms, the proposed knee supports first principles evaluation and potential transfer of natural human gait for efficient robot walking. A simple and low cost design promotes mass replication and widespread adoption within the robotics community.

A basic kneed walker could be modelled as a planar biped depicted in Figure 3. An upper body linkage manipulates robot center of mass (CoM) in the sagittal plane to initiate gait. Such configuration biomimics human physiology and can be considered as a template in biped robotics development. Although different postures during walking are possible, the most fundamental gait in Figure 2 provides a basis for which variations could be built upon. Under these

¹Cheng-Yueh Liu, Jaspreet S. Dhupia, and Minas Liarokapis are with the Department of Mechanical and Mechatronics Engineering, The University of Auckland. Emails: cliu695@aucklanduni.ac.nz, j.dhupia@auckland.ac.nz, minas.liarokapis@auckland.ac.nz

²Pei-Chun Lin is with the Department of Mechanical Engineering, National Taiwan University, Taiwan, ROC. Email: peichunlin@ntu.edu.tw

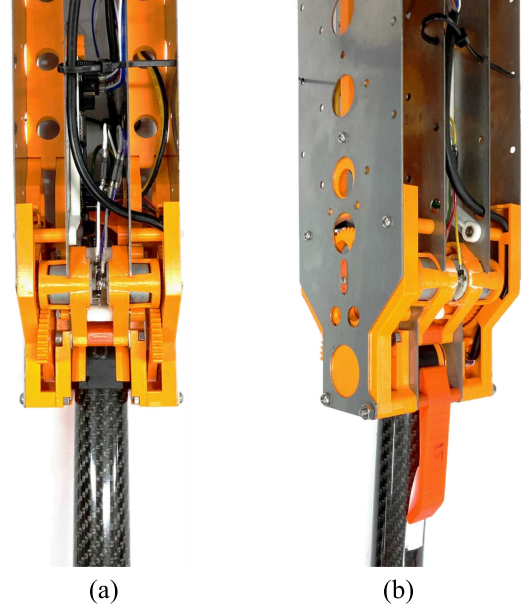


Fig. 1. The proposed knee joint assembly. Subfigure a) presents the rear view and subfigure d) presents the isometric view. All associated mechanisms, actuators, and electronics presented throughout the paper are integrated within the depicted assembly. The near symmetrical layout across both sagittal and coronal planes, facilitates an even distribution of inertia and mass.

circumstances, the knee of stance (dotted) leg remains locked and rigid.

Therefore, the sole purpose for knee bends of the rear swing leg is preventing foot scuffing. Such gaits do not require knees to exert much torque (if any) requiring little actuation. This effect is further accentuated should lower limb extremities, consisting of shank and foot, possess minimal mass and rotational inertia about the knee.

The Lagrange dynamic model describing biped motion of the configuration in Figure 3 is found to be

$$D(\theta)\ddot{\theta} + h(\theta, \dot{\theta}) + G(\theta) = \tau \quad (1)$$

where

$$\left. \begin{aligned} \theta &= [\theta_1, \theta_2, \dots, \theta_5]^T, \\ \tau &= [\tau_{\theta_1}, \tau_{\theta_2}, \dots, \tau_{\theta_5}]^T, \\ h(\theta, \dot{\theta}) &= \text{col} \left[\sum_{j=1(j \neq i)}^5 h_{ijj}(\dot{\theta}_j)^2 \right], \\ G(\theta) &= \text{col}[G_i(\theta)], \\ D(\theta) &= [D_{ij}(\theta)], \quad i, j = 1, 2, \dots, 5. \end{aligned} \right\} \quad (2)$$

Here $D(\theta)$ is the 5×5 symmetric, positive definite

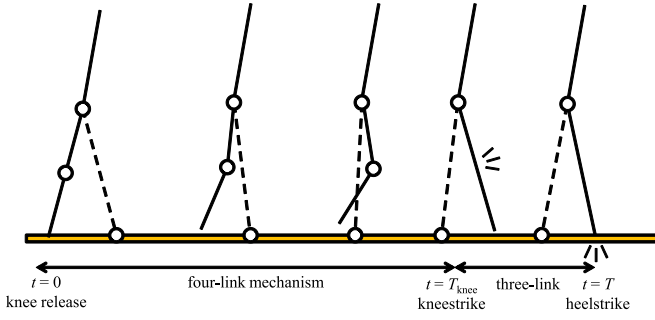


Fig. 2. Walking gait cycle for a multi-link planar biped model. The first phase occurs after foot lift-off until kneestrike (operating as four links), and the second phase continues until heelstrike as a two-link mechanism.

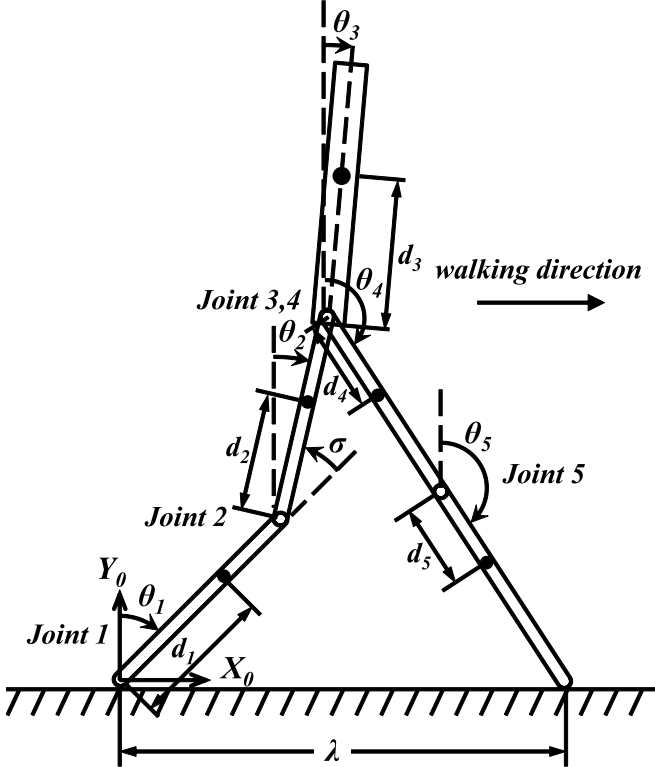


Fig. 3. Nomenclature of a 5-link planar biped robot suitable for the proposed knee joint. By manipulating upper body angle θ_3 , the robot can commence walking when center of mass is ahead of stance (front) foot.

inertia matrix, $h(\theta, \dot{\theta})$ is the 5×1 vector of centripetal and Coriolis forces, $G(\theta)$ is the 5×1 vector representing gravitational forces, and τ is the 5×1 generalized torque vector corresponding to θ_i . A full derivation [1] and equations during heel and knee strike switching events [2] are well documented.

Figure 4 portrays generalised knee angles, which never exceed -70° , during comfortable human walking and compares that with various biped setups. Physiologically, the human knee does undergo slight flexion during stance. Passive dynamic walkers can be classed as legged machines for which dynamic walking occurs naturally. By offering a clutch for transmission engagement and disengagement, natural bipedal dynamics can be combined easily with active energy input so as to produce efficient and versatile walking over

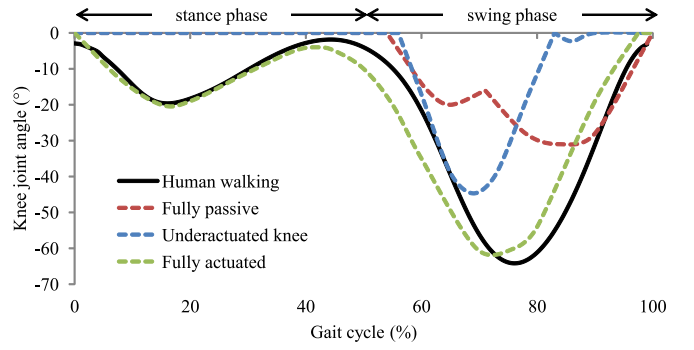


Fig. 4. Representative knee angles of human vs select biped robot topologies during walking. Flexion angles are negative. Comfortable human walking speed = 1.24 m/s, stride length (2λ) = 1.32 m. Graph constructed as a composition from existing graphs in [3]–[5]; human knee flexion angles collated using averages of comfortable gait data in [6].

a broad range of unstructured terrains [7]. Another category of simple walking machines, underactuated bipeds, can take advantage of upper-body control, resulting in efficient limit-cycle gaits by avoiding generation of negative input power [8]. Moreover, robots that harness passive dynamics use less control and energy than other powered robots, yet walk more naturally [9]. Through actively controlling the hip, knee joints can be underactuated during the locomotive gait. Previous underactuated or passive dynamic walkers lock their knees straight throughout stance phase. Table I provides an overview of knee functionalities in fully passive, underactuated and fully actuated biped setups. In [10] Etoundi, et al. reviewed various biomimicking knee joints and identified general trends. For example, a bio-inspired knee joint incorporated planetary gearing with pneumatic artificial muscles actuating a compound sun gear pulley [11]. Another design consists of a crossed four-bar linkage with variable transmission and a joint stop proposed in [12].

The remainder of this paper is organized as follows: Section II divulges on the inspiration behind the mechanical design, Section III discusses in detail how the proposed transmission mechanism works and custom electronics, Section IV presents the experimental validation of the efficiency of the proposed knee assembly, while Section V concludes the paper and discusses future directions.

II. DESIGN INTENT

A disengageable transmission facilitates controlled passive walking. For the most elementary geared knee clutch, the decoupling of joints to any actuation transmission enables underactuation and exhibit passive dynamics [19]. Such natural movements form an ideal scenario whereby a robot could harness the ultimate manifestation of energy efficiency, coupled with a fully actuated or backdrivable joint when necessary.

Hip joint actuation is by far the main power contributor for sustaining forward gait locomotion [8], [9]. In this context, it is feasible to derate (or underpower) the knee joint as much as possible. The knee need not contribute torque for forward motion and can be locked during stance. Positioning the knee

TABLE I
VARIOUS KNEE ACTUATION TOPOLOGIES FOR A HUMAN-INSPIRED WALKER.




Type	Fully passive	Underactuated knee	Fully actuated
Example image			
Description	Passive dynamic walkers walk down slope without any actuation. Powered by gravity.	Robot with passive-inspired elements and actuated hip. Walks on flat surface.	All relevant degrees of freedom are actively controlled with actuators, including knees and hip joints.
Select examples	Dexter, robots by Garcia/McGeer, Ruina/Collins [3], [7], [9]	Dribbel, Denise [13], [14]	ASIMO, Atlas, NAO, Veronica, RoK-4 etc. [15]–[17]
Knee design	No active actuation. Knee flexion/extension occurs naturally during gait.	Active knee locking mechanism. Knee rotation not actuated.	Knee joint directly actuated via permanent transmission. May use adaptable or compliant joints. [18]
Angle range	0° to -35° typ	0° to -50° typ	0° to -65° typ
Knee torque performance	0 Nm	0 Nm	Varies greatly depending on robot.
Knee lock	May incorporate passive knee locking mechanism for stance phase.	Electromagnetic, voice-coil, motor or solenoid driven etc.	Under-actuated examples plus clutch variations coupled to active transmission.
Passive mode	Yes	Yes	No
Controllable flexion	No	No	Yes

TABLE II
KNEE DESIGN SUMMARY AND PHYSICAL PARAMETERS OF TEST SHANK.

	Variable	Value
Angle range	$-\sigma$	0° to -70°
Knee lock		Latching solenoid
Mechanism mass		470 g
Passive mode		Yes
Controllable flexion		Yes
Shank length	$d_1 + d_5$	0.45 m
Shank mass	(Link 1)	0.09 kg
Foot mass	Joint 1	0.04 kg
Moment of inertia about knee		0.0142 kg m ²
Shank CoM	d_1	0.1558 m

actuators nearer the hip with mechanisms, such as linkages or cables, for transmission [20] add complexity and mass. A lightweight knee joint reduces overall leg mass and inertia, which facilitates smaller hip joint torque requirements.

During the stance phase, each knee must be able to support its corresponding thigh, hip, and swing leg without bending. Such substantial loading would require knee exertion of significant torques during what should be a passive gait phase.

One straightforward actuation methodology is to mount a geared, inline motor directly at the knee joint with supporting elastic and damping elements [21]. However, with no locking mechanisms, energy is consumed to oppose bending torques using the employed actuator. Instead of relying on actuators, a separate knee locking mechanism, which does not consume energy to maintain state, is desirable. Plooi, et al. [18] identified properties an ideal robot joint locking device shall possess: i) adjustable locking directions, ii) ability to unlock while under load, iii) low energy consumption, iv) ability to lock in any position, v) short switching time, vi) high locking force and vii) be compact, lightweight, and inexpensive. Locks could be categorized by active or passive modes of operation, which include electromagnetic [22], permanent magnet [23] or the use of suction cups for lock activation. Reynolds [24] developed a differential-brake style clutch. However, passive knee locking mechanisms could lose synchronization with the gait cycle that can affect overall reliability.

III. MECHANISM DESIGN

A large speed reduction ratio is necessary to provide sufficient torque for actuating robot shanks [25]. The solution presented here uses a multistage gear reduction system incorporating a compound gear for an overall 40:1 gear reduction. The hardware is composed of subsystems incorporating a gearbox, lock, associated electronic drivers, and a rotary encoder (see Figure 5). The knee joint is actuated using

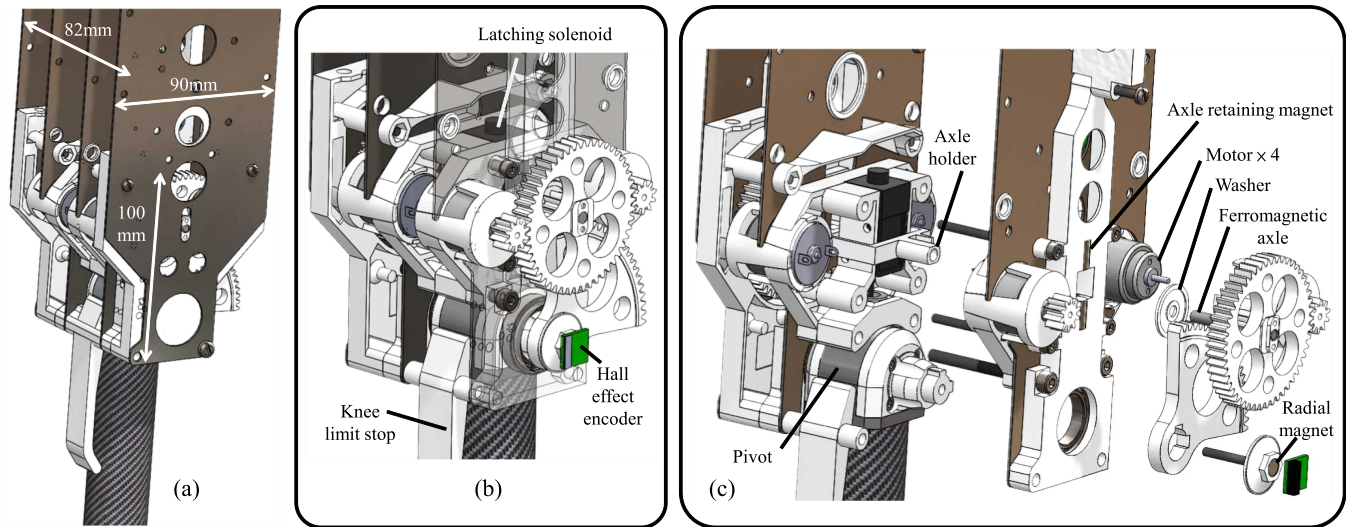


Fig. 5. Knee joint mechanism. Mass is 470g excluding chassis components. a) Overview. b) Cutaway view without side sheetmetal. c) Exploded view of left half, revealing axle holder, which can translate vertically about the latching solenoid in the inner core. Mechanism is symmetrical about sagittal plane.

a modified planetary gearbox transmission system that can be disengaged for passive dynamics. An embedded bolt, powered by a bistable or latching solenoid, keeps the shank either locked at a fixed angle (during stance phase) or unlocked without consuming any energy to maintain state (see Figure 6).

Serial elastic actuation elements were considered but omitted. Low transmission torque outputs mean elastic components must be soft, implying minuscule energy storage is obtainable. However, damping elements could be retrofitted to smooth stroke transitions at end limits.

A. Gearbox

In the proposed design, Type 140 brushed direct current (DC) motors, rated at 6V (Mabuchi RE140RA-12240 or equivalents), provide knee joint power at 80 g each. Four motors are arranged in a planetary fashion as depicted in Figure 6, without ring gear. Coupled to a compound sun gear, the two-stage transmission imparts a gear reduction of 50:10 and 80:10 respectively. Furthermore, each pair of motors is symmetrically positioned in both the sagittal and transverse planes. This deliberate organization ensures the mechanism imparts identical inertial distribution across both planes while promoting equal torque contribution from each motor.

B. Gearbox Doubles as Clutch

Each compound (sun) gear revolves between two, significantly smaller, planet gears placed diametrically opposite and horizontally 180° apart. Rotating the compound gear about a fixed axle transmits torque to bend the knee in either direction, which is achieved by synchronous operation of all four DC motors in tandem and rotating the joint. However, the transmission is deliberately designed so other modes of operation are possible if minor constraints are removed. When the sun gear axle is permitted to translate vertically upwards, by a lateral displacement marginally greater than the gear tooth depth, the compound gear is

decoupled from the output (second gear set). This additional degree of freedom can be employed by contra-rotating the two planets in opposite directions. It is important to ensure the sun gear movement is restrained such that the teeth always mesh with planet gears. Therefore, four modes of operation become possible: i) transmission disengagement, ii) transmission engagement, iii) clockwise joint actuation, and iv) counterclockwise joint actuation. Retaining the sun gear axle in the up or down position, for transmission disengagement or engagement respectively, can be achieved by any methodology deemed suitable in the actual application. For the purposes of this paper, permanent magnets are used in conjunction with a ferromagnetic axle. The two motors could also impart net up or down translational forces so as to assist in retaining the sun gear position. For example, when the axle is in down (engaged) position for knee rotation, both planet gears (and motors) are actuating in the same direction. Due to being positioned opposite each other, one of the planets will be invoking an upwards force when driving the sun gear teeth, but neutralized by the other planet exerting force downwards. By applying not only various voltages or duties, but also a differential, to the two motors while actuating the joint, both the net output torque and sun gear retaining force can be adjusted. By repurposing the very motors and gears used for joint actuation, the gearbox effectively doubles as a clutch. Simple yet innovative supplementary mechanics are important when pursuing elegant outcomes.

C. Joint Lock

Electromagnets or voice-coil actuated locks [13] consume substantial current (up to a few amperes) just to maintain state. A miniature latching solenoid (Shih Shin SH-K0730S-06V) [26] was identified so as to implement a linear bolt-lock configuration. These devices passively maintain a set position without constant application of electrical current. The latching solenoid linearly actuates a $\varnothing 6.3$ mm bolt into the joint pivot, with 9 mm stroke for locking (Figure 6c).

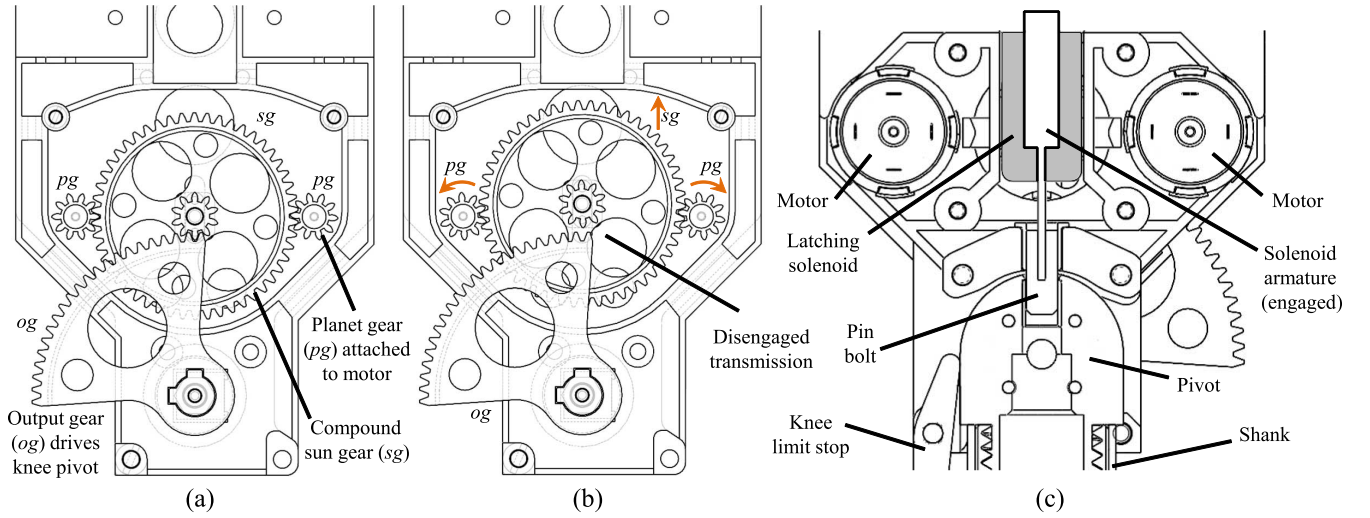


Fig. 6. Gearbox and knee lock. a) Engaged transmission; compound sun gear (sg) is down and mating with output gear (og) of knee pivot. b) Disengaged transmission; sg is up and floats above og . c) Knee lock mechanism with pin bolt engaged, preventing the pivot from rotating. The cross section is across lower limb sagittal plane.

TABLE III

KNEE DRIVER LOAD CURRENT ESTIMATION FOR SELECTED R_{FB} .

R_{FB}	a_{ADC} (10^{-3})	b_{PWM}	c_{const} (10^{-3})	R^2	RMSE (10^{-3})	RSE (10^{-3})
4k7	1.09244	0.23724	-10.9677	0.9972	4.6597	4.8732
10k	0.52400	0.17088	-7.80886	0.9997	0.9922	1.0501
22k	0.24959	0.24924	2.80037	0.9997	1.1807	1.2623

To minimize friction and assist engagement, the pivot is press-fitted with an IGUS® H370SI-0405-06 self lubricated bushing which acts as the receptacle. A secondary IGUS® H370FI-0405-06 bushing supports the bolt on the fixed side. In practice, the fully assembled joint exhibits a maximum backlash of approximately 5° when locked. Liu, et al. [27] devised a tapered pin lock configuration, the shape of which removes fit clearance to prevent knee bending when engaged. Such provision for compliance is a reference for further mechanical refinements.

In order to actuate the aforementioned electromechanical DC motors and solenoids, custom made knee driver electronics have been developed. Programmable resistor/capacitor combinations, as described in the evaluation section below, generate voltages that estimate feedback current sensing characteristics of the four DC motors. An 8-bit analogue to digital converter (ADC) reads the associated voltage. Both the PWM generator IC and ADC employ I2C for data communications with the microcontroller unit. Finally, a 14 bit Hall-effect rotary encoder (AS5048) about the knee joint axis of rotation measures knee stance angle. A radial magnet is placed on one end a rotating axle (hidden), adjacent to the encoder. I2C interface is used throughout for bus commonality.

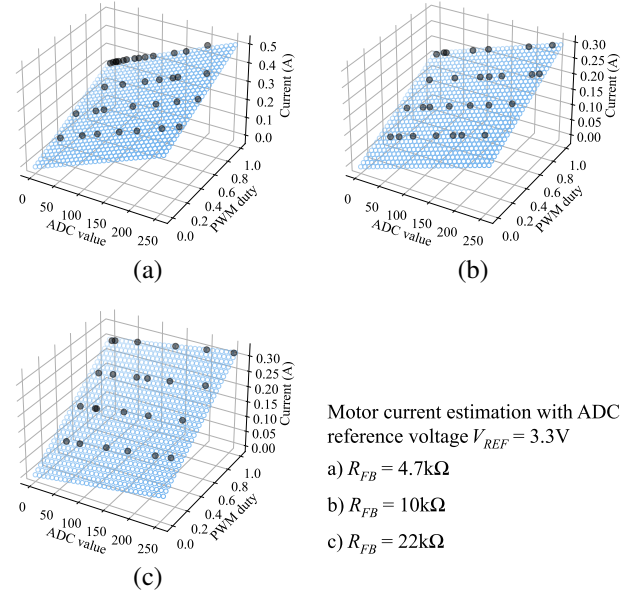


Fig. 7. Knee driver current sensing calibration with various feedback resistors (R_{FB}). By choosing an appropriate value, full scale detection of motor current can be realized.

IV. EVALUATION

The proposed knee joint assembly is depicted in Figure 1. The shank (attached to the joint) is a carbon-fiber tube with a plastic “shoe” (see Figure 10). Apart from electromechanical actuators, knee pivot and bolt lock, all other mechanical parts are printed with fused deposition modeling using polylactic acid (PLA). Shank parameters and knee joint costings are listed in Tables II and IV respectively.

A. Motor Driver and Current Sensing

The knee motor driver PCB incorporates 8-bit current sensing capabilities. Current sensing calibration is required

TABLE IV
LISTED COST BREAKDOWN FOR ONE KNEE MECHANISM.

Item	USD
PLA material	2
DC motors (four)	8
Latching solenoid	12
SS304 lock pin bolt (CNC)	30
AL7075 knee pivot (CNC)	180
Bearings	15
Electronics	60
Miscellaneous	5
Total	312

to understand the relationship between ADC readings, H-bridge PWM duty cycles, and actual (motor) load current for programmable current sensing resistor values (R_{FB}). In this paper, tests were conducted with 1526Hz PWM frequency and slow decay (low side active freewheeling). Variable loads are connected directly to one knee driver H-bridge output with a multimeter in series. Results for $R_{FB} = 4.7k$, 10k and 22k Ω are depicted in Figure 7.

Optimal R_{FB} selection should produce full-scale ADC readings (0 to 255) across a range of expected load currents. For each scenario, a multiple linear regression is conducted by treating ADC value, PWM duty and load current as independent variables. Table III lists the multiple linear regression results including correlation coefficients:

$$I_{load} = a_{ADC}ADC + b_{PWM}PWM + c_{const} \quad (3)$$

where I_{load} , ADC and PWM are the measured load current, raw ADC values and PWM duty cycle respectively. Selecting a sensible R_{FB} value necessitates coordination with experimental gait requirements to be conducted in the future.

B. Joint Lock

The latching solenoid disengagement is provided by compression springs. When compressed, these must exert less force than the solenoid's 8 N permanent magnet latching force. Liberal lubrication is applied to lock contact surfaces, which is necessary for successful operations. Unimpeded lock transition takes roughly 0.2 s.

1) *Unlocking*: During disengagement, maximum spring (ejection) force occurs when there is net zero magnetic flux in the solenoid armature, which is afforded by a reverse current of 1 A at 8 V. Please note that there is some backlash between the bolt and the receptacle. During level walking, knee unlocking and bending only occurs during swing phase and the motors never need to overcome torque, induced by weight above the joint, in the locked stance phase.

2) *Locking*: On the contrary, a larger forward current results in greater interim latching force for compressing the

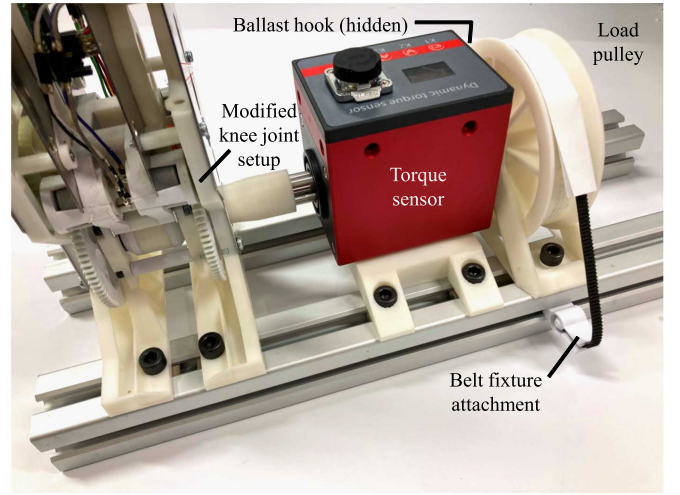


Fig. 8. Knee joint torque evaluation setup. A CALT DYN-200 sensor is serially attached to the output of a modified joint setup. Load pulley and ballast weight acts as friction device for generating resistive torque.

spring. Therefore, maximum current can be applied for the shortest duration possible. In practice, lock activation during joint rotation means that the bolt rubs against the pivot until it engages the receptacle upon alignment. Heat dissipation should be alleviated. In order to maximize their active duty, solenoids should be mounted to the chassis via a thermally conductive bracket.

C. Gearbox Clutch Mode

Given appropriate motor driver commands, various function modes can be triggered as intended. An important observation is that sun gear dislodgement can occur if there is sufficient obstruction that impedes free rotation of the joint output. This means that transmission could be automatically disengaged if knee joint fails to turn during gear rotation, which is an unintentional consequence of the selected design. Thus, the sun gear must be adequately retained with sufficient locking force to prevent unintended decoupling during operation. Methods that could be employed include selecting suitable spring clips and permanent magnets.

D. Torque Performance

Certain modifications are conducted for mounting a duplicate device onto a torque test rig (see Figure 8). Instead of rotating a shank, one end of a CALT DYN-200 torque sensor is directly coupled to the output of the knee joint. The other end is connected to a torque load generator. A $\varnothing 110$ mm pulley, supporting ballast off a belt, is attached as the load. One end of the belt wraps around the pulley and is fixed to the setup frame. A piece of 80 gsm photocopy paper envelops the belt at the pulley contact area. By changing ballast mass hanging off the belt, the radial and friction force and hence resistive torque from the paper-pulley interface is varied. In order to maintain consistent load torques, the pulley is rotated in the direction that prevents upward force being exerted on the ballast.

Reasonable PWM duties at 24 V were applied to the motor driver board. Various speed-torque performances are depicted

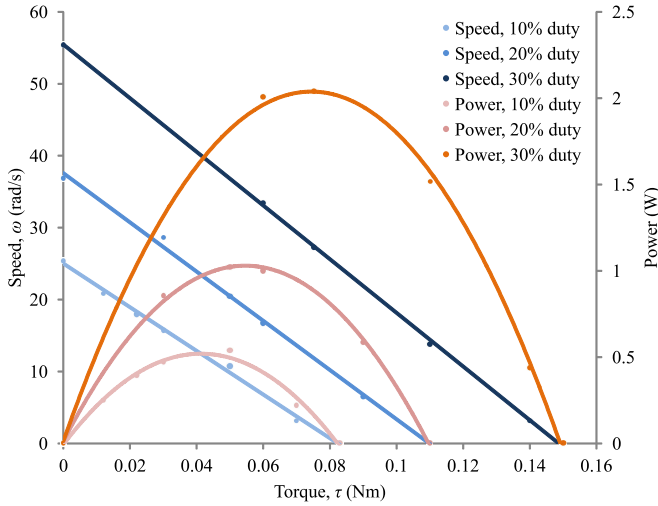


Fig. 9. Knee joint performance under various loads. Duty cycles up to 30% were evaluated, which gives an acceptable range of speed-torque characteristics.

TABLE V
JOINT PERFORMANCE LINEAR REGRESSION ESTIMATION.

Duty (%)	$\frac{\Delta\omega}{\Delta\tau}$ ($\frac{\text{rad}}{\text{Nm s}}$)	$\omega_{\tau=0}$ (rad/s)	R ²	RMSE	RSE
10	-303.37124	25.00549	0.9965	0.5125	0.6064
20	-342.23120	37.57943	0.9975	0.6214	0.7610
30	-373.02770	55.46222	0.9996	0.3811	0.4668

and listed in Figure 9 and Table V respectively. Steady state readings between trials are logged. The setup was left to cool down at room temperature for a minute after each trial. Furthermore, the ballast load is removed and reset between trials to mitigate steady state error.

The system essentially consumes a constant current (at 24 V) regardless of speed/torque for each duty (10%, 0.85 A; 20%, 1.68 A; 30%, 2.6 A). Substantial energy overheads may be present as a constant cost of actuation in the transmission setup, suggesting limited system efficiency.

E. Knee Rotation

The knee, installed into a robotic lower limb assembly, is verified with a proportional-integral-derivative (PID) controller running at 20 Hz. The leg thigh is fixed horizontally for reference and all knee joint angles are measured in degrees and clockwise relative to fully extended shank position (see Figure 10). Sample test scenarios are depicted in Figure 11. Given prescribed gains, the setup is capable of attaining 0.6 s settling time between -67° and -27° with 2° steady state error. This corresponds to 40° flexion from a combined swing and stance angle of 23° in gait without considering thigh dynamics during walking. In bipeds, hip actuation during leg swings passively contributes to shank dynamics in an underactuated manner. Test results demonstrate the feasibility of employing the knee joint design in a biped and warrants further development. Results suggest the following:

- Based on knee angle during the proposed gait cycle (Figure 4), the flexion range of proposed knee mechanism meets or exceeds performance of comparable passive or underactuated walkers. However, in practice, any flexion angle is permissible as long as foot scuffing is avoided.
- Torque requirements are sufficiently small to swing the lightweight shank, which limits the loading imparted on knee actuation and supports rapid flexion or extension.

F. Open-Source Dissemination

All the files that allow replication of the multi-modal, selectively lockable, compact, affordable knee joint assembly are publicly available at the following URL:

<https://github.com/Cheng-Yueh/knee>

A video demonstration of the performance of the proposed knee assembly can be found at the following URL:

https://youtu.be/-a_vLSxSMBE

V. CONCLUSION AND FUTURE WORK

In this paper, various typologies of active knee joints developed for biped robots were reviewed. Desirable characteristics include options for both active and passive modes of joint operation, lightweight mechanisms, and a disciplined strategy to lock and unlock the knee during swing phase. Ideally, the latter offers active toggling but maintains state without energy consumption. The capability of arbitrarily (dis)engaging transmission can be used to fulfil passive dynamic inspired humanoid gait where possible, while permitting controlled knee actuation when necessary. This unique capability can promote natural gait development for research in efficient biped robots.

These traits form a minimalistic and novel solution for enabling passive, underactuated and driven capabilities that remains locked during stance phase. A multistage arrangement with planet gears provides not only joint rotation, but also acts as a clutch that can actively engage or disengage transmission. In lieu of electromagnets or passive suction cups, latching solenoids offer a knee lock solution that can be actively toggled without consuming current to maintain state. Together, these modular integrations manifests many ideal attributes a biped robot knee joint should possess.

Knee joint validation on a walking bipedal robot will be necessary. Locking performance, like anti-moment torque capability, energy consumption details, and options to lock at arbitrary angles demands evaluation. Fine tuning mechanical elements, incorporating dampers, and motor driver parameters is essential for improving energy efficiency. Opportunities remain in refining closed-loop methodologies beyond the rudimentary PID controller presented. The design deliberately facilitates underactuation for controlled yet efficient biped walking in future development.

ACKNOWLEDGMENT

This work is partially supported by the National Science and Technology Council, Taiwan, under contract: MOST 110-2221-E-002-111-MY3.



Fig. 10. Side view of a complete assembled robot leg that incorporates the proposed knee assembly. The thigh is fixed horizontally such that the shank is free to swing. A carbon fiber tube is used for the leg development while the knee assembly uses a combination of metal and 3D printed parts.

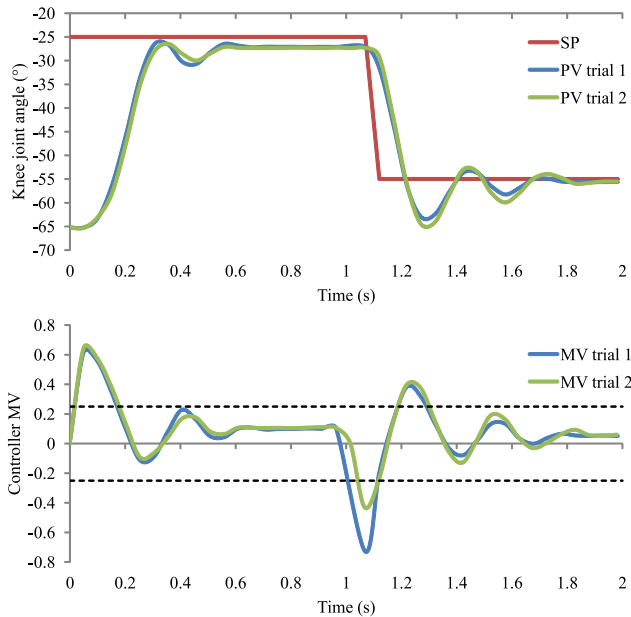


Fig. 11. Knee-shank actuation with PID (k_p , k_i , $k_d = 0.015$, 0.008 , 0.00125). Set point (SP), present value (PV) knee joint angles and controller outputs (MV) are plotted. MV clipped to ± 0.25 for PWM duty.

REFERENCES

- [1] S. Tzafestas, M. Raibert, and C. Tzafestas, "Robust sliding-mode control applied to a 5-link biped robot," *Journal of intelligent & robotic systems*, vol. 15, no. 1, pp. 67–133, 1996.
- [2] E. Borzova and Y. Hurmuzlu, "Passively walking five-link robot," *Automatica (Oxford)*, vol. 40, no. 4, pp. 621–629, 2004.
- [3] K. Rushdi, D. Koop, and C. Q. Wu, "Experimental studies on passive dynamic bipedal walking," *Robotics and Autonomous Systems*, vol. 62, no. 4, pp. 446–455, 2014.
- [4] V. Duindam and S. Stramigioli, "Modeling and control for efficient bipedal walking robots - a port-based approach," *Springer Tracts in Advanced Robotics*, vol. 53, p. 156, January 2009.
- [5] A. Maiorino and G. G. Muscolo, "Biped robots with compliant joints for walking and running performance growing," *Frontiers in Mechanical Engineering*, vol. 6, 2020.
- [6] R. Senden, R. Marcellis, P. Willems, M. Witlox, and K. Meijer, "Normative 3d gait data of healthy adults walking at three different speeds on an instrumented treadmill in virtual reality," *Data in Brief*, vol. 53, p. 110230, 2024.
- [7] T. McGeer, "Passive dynamic walking," *The International Journal of Robotics Research*, vol. 9, no. 2, pp. 62–82, 1990.
- [8] F. Asano, "High-speed stealth walking of underactuated biped utilizing effects of upper-body control and semicircular feet," in *2018 IEEE/RSJ International Conference on Intelligent Robots and Systems (IROS)*. IEEE Press, 2018, p. 4375–4380.
- [9] S. Collins, A. Ruina, R. Tedrake, and M. Wisse, "Efficient bipedal robots based on passive-dynamic walkers," *Science*, vol. 307, no. 5712, pp. 1082–1085, 2005.
- [10] A. C. Etoundi, C. L. Semasinghe, S. Agrawal, A. Dobner, and A. Jafari, "Bio-inspired knee joint: Trends in the hardware systems development," *Frontiers in Robotics and AI*, vol. 8, 2021.
- [11] Y. Liu, X. Zang, Z. Lin, X. Liu, and J. Zhao, "A bio-inspired knee joint for biped robots," in *2016 IEEE International Conference on Information and Automation (ICIA)*, 2016, pp. 1387–1391.
- [12] K. Ueki, R. Sato, A. Ming, M. Shimojo, M. Hammadi, and J.-Y. Choley, "Development of knee joint mechanism with variable transmission and joint stop for bipedal robot inspired by human structure," in *2020 21st International Conference on Research and Education in Mechatronics (REM)*, 2020, pp. 1–6.
- [13] G. van Oort, R. Carloni, D. J. Borgerink, and S. Stramigioli, "An energy efficient knee locking mechanism for a dynamically walking robot," in *2011 IEEE International Conference on Robotics and Automation*, 2011, pp. 2003–2008.
- [14] S. Anderson, M. Wisse, C. Atkeson, J. Hodgins, G. Zeglin, and B. Moyer, "Powered bipeds based on passive dynamic principles," in *5th IEEE-RAS International Conference on Humanoid Robots*, 2005, pp. 110–116.
- [15] T. Mikolajczyk, E. Mikolajewska, H. F. N. Al-Shuka, T. Malinowski, A. Kłodowski, D. Y. Pimenov, T. Paczkowski, F. Hu, K. Giasin, D. Mikolajewski, and M. Macko, "Recent advances in bipedal walking robots: Review of gait, drive, sensors and control systems," *Sensors*, vol. 22, no. 12, 2022.
- [16] Y. Huang, B. Vanderborght, R. Van Ham, Q. Wang, M. Van Damme, G. Xie, and D. Lefeber, "Step length and velocity control of a dynamic bipedal walking robot with adaptable compliant joints," *IEEE/ASME Transactions on Mechatronics*, vol. 18, no. 2, pp. 598–611, 2013.
- [17] M.-H. Park and B.-K. Cho, "Design of new drive mechanism for dynamic movement of humanoid robot legs," in *2023 IEEE-RAS 22nd International Conference on Humanoid Robots (Humanoids)*, 2023, pp. 1–8.
- [18] M. Plooijs, G. Mathijssen, P. Cherelle, D. Lefeber, and B. Vanderborght, "Lock your robot: A review of locking devices in robotics," *IEEE Robotics & Automation Magazine*, vol. 22, no. 1, pp. 106–117, 2015.
- [19] A. G. Baines, "Knee design for a bipedal walking robot based on a passive-dynamic walker," BSc report, Massachusetts Institute of Technology, 2005.
- [20] J. Reher, W.-L. Ma, and A. Ames, "Dynamic walking with compliance on a cassie bipedal robot," *2019 18th European Control Conference (ECC)*, pp. 2589–2595, 2019.
- [21] D. J. Braun, J. E. Mitchell, and M. Goldfarb, "Actuated dynamic walking in a seven-link biped robot," *IEEE/ASME Transactions on Mechatronics*, vol. 17, no. 1, pp. 147–156, 2012.
- [22] K. B. Trifonov, G. Enriquez, and S. Hashimoto, "Design issues and applications for a passive-dynamic walker," in *International Conference on Multimedia and Ubiquitous Engineering*, 2009.
- [23] K. B. Trifonov and S. Hashimoto, "Active knee-release mechanism for passive-dynamic walking machines and walking cycle research," in *2008 IEEE/RSJ International Conference on Intelligent Robots and Systems*, 2008, pp. 179–184.
- [24] A. A. A. Reynolds, "Design and control of a clutch for a minimally-actuated biped based on the passive-dynamic simple walker," BSc report, Massachusetts Institute of Technology, 2006.
- [25] RE-140RA, Mabuchi Motor Co., Ltd, 2020. [Online]. Available: https://www.mabuchi-motor.co.jp/motorize/branch/motor/pdf/re_140ra.pdf
- [26] SH-K0730S, Shih Shin Technology Co., Ltd., 2023. [Online]. Available: <https://www.solenoids.com.tw/document-detail/0/product-data-SH-K0730/>
- [27] X. Liu, X. Zang, Y. Zhu, Y. Liu, and J. Zhao, "System overview and walking dynamics of a passive dynamic walking robot with flat feet," *Advances in Mechanical Engineering*, vol. 7, no. 12, p. 1687814015620967, 2015.